Dynamic Properties of the Tetrahydrofuran Clathrate Hydrate, Investigated by Solid State ^{2}H NMR Spectroscopy

Marta Bach-Vergés, Simon J. Kitchin, and Kenneth D. M. Harris*

School of Chemistry, University of Birmingham, Edgbaston, Birmingham B15 2TT, United Kingdom

Minjas Zugic and Carolyn A. Koh*

Department of Chemistry, King's College London, Strand, London WC2R 2LS, United Kingdom

Received: July 18, 2000; In Final Form: January 26, 2001

Clathrate hydrates are solid inclusion compounds in which cages formed by a water host structure accommodate guest molecules of appropriate size and shape. Dynamic properties of the clathrate hydrate containing tetrahydrofuran (THF) guest molecules have been investigated using solid-state ^{2}H NMR techniques, including line shape analysis and spin−lattice relaxation time (T_1) measurements. ^{2}H NMR results for THF−D_2O suggest that there are at least two dynamically distinguishable types of water molecule, both undergoing four-site tetrahedral jump motions but with different rates. The population ratio may be assigned as 3:1, consistent with the known crystal structure. Above 193 K, the dynamics of both components are in the intermediate motion regime (10^{-7} s $\lesssim \tau_c \lesssim 10^{-3}$ s). From analysis of the ^{2}H NMR line shapes, the jump rates have been determined as a function of temperature, and activation parameters have been estimated. The ^{2}H NMR spectrum for THF-d_8−H_2O comprises a single line, which broadens and changes shape on decreasing temperature. These observations are interpreted in terms of the THF-d_8 guest molecules undergoing an approximately isotropic motion in the rapid regime ($\tau_c \lesssim 10^{-7}$ s), but with a distribution of slightly anisotropic characteristics. As the guest molecules reorient rapidly in comparison with the dynamics of the water molecules, different guest molecules are effectively surrounded by structurally different water cages so that there is a distribution in terms of the anisotropic characteristics associated with the reorientational motions of different guest molecules. These conclusions are complemented by information determined from ^{2}H NMR spin−lattice relaxation time measurements.

1. Introduction

Clathrate hydrates, first discovered by Davy in 1811,[1] are a class of solid inclusion compounds in which cages formed by a water host structure accommodate guest molecules of appropriate size and shape.[2−4] In addition to fundamental research on the preparation, stoichiometry, thermodynamic properties, crystal structure, and dynamic properties of clathrate hydrates, these materials also have considerable technological interest. For example, the formation of clathrate hydrates in natural gas pipelines and in marine sediments has created much interest in recent years, and applications in fractionation and storage of gases have also been proposed. Currently, there is considerable interest[2,5,6] in understanding the formation and growth of clathrate hydrates, particularly because the formation of these materials in pipelines during the production and transmission of natural gas and petroleum poses problems for the gas and oil industries.

The crystal structures of most clathrate hydrates can be classified into two types, denoted structures I and II.[7,8] In both cases, the water molecules form polyhedral cages held together by O−H···O hydrogen bonds. At least 120 different types of guest species are known to form clathrate hydrates with structure types I or II. Other structures of clathrate hydrates have also been reported.[9,10]

In this paper, we focus on the clathrate hydrate containing tetrahydrofuran (THF) guest molecules. The THF clathrate hydrate has the type II structure[11] (cubic, $Fd\bar{3}m$, $a = 17.3$ Å), comprising 16 pentagonal dodecahedral cages and 8 hexadekaidecahedral cages connected by their pentagonal faces. The two types of cage are shown in Figure 1. The pentagonal dodecahedral cage has 12 pentagonal faces, and the average radius is 3.9 Å. The hexadekaidecahedral cage has 12 pentagonal faces and 4 hexagonal faces, and the average radius is 6.6 Å—as the actual radius fluctuates by only about 2% from this average value, this cage is almost spherical. Only the hexadekaidecahedral cages are sufficiently large to accommodate THF guest molecules, for which the effective molecular diameter is about 5.9 Å,[11,12] and the smaller pentagonal dodecahedral cages are empty. The large and small cages are constructed from 28 and 20 water molecules, respectively. Each water molecule forms hydrogen bonds to three neighbors within the cage wall and to one neighbor outside the cage. The O···O distances range from 2.72 to 2.76 Å, and the O···O···O angles are close to the tetrahedral angle (the average deviation from the tetrahedral angle is 3.0°). There are three independent types of water molecule in the asymmetric unit, and the sites occupied by the oxygen atoms of these water molecules have point symmetries $\bar{4}3m$, $3m$, and m (multiplicities 8, 32, and 96 respectively). X-ray and neutron diffraction studies[11,13] suggest that the hydrogen

* Corresponding authors. K.D.M.H.: e-mail, K.D.M.Harris@bham.ac.uk; phone, +44-121-414-7474; FAX, +44-121-414-7473. C.A.K.: e-mail, carolyn.koh@kcl.ac.uk; phone, +44-207-848-2380; FAX, +44-207-848-2810.

10.1021/jp002529o CCC: $20.00
Published on Web 03/16/2001

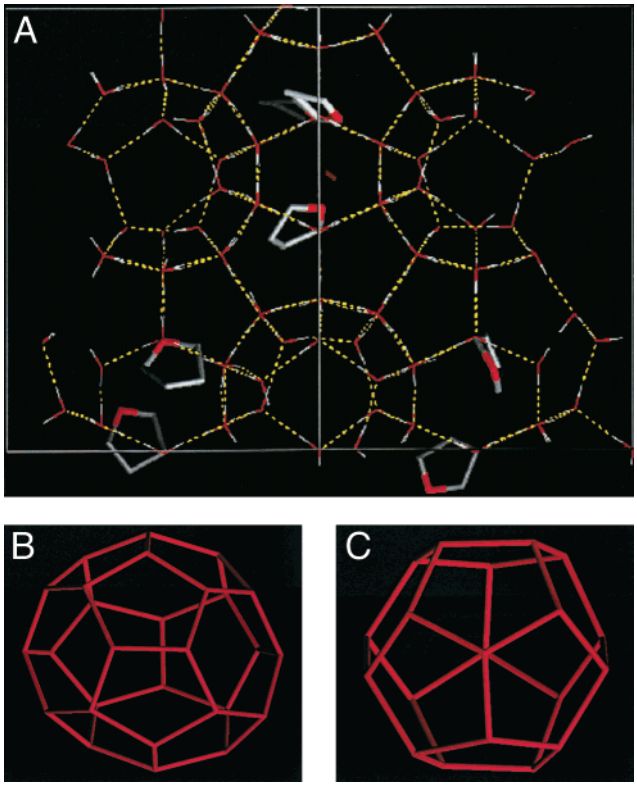

Figure 1. Structure of the THF clathrate hydrate, showing (a) THF molecules occupying the large water cages (in arbitrary positions), and the structures of (b) the large hexadekaidecahedral cage and (c) the small pentagonal dodecahedral cage.

atoms of the water molecules are disordered over two positions in each O···O hydrogen bond. Results from dielectric spectroscopy,[14,15] solid-state ^{1}H NMR,[16] solid-state ^{2}H NMR,[17] adiabatic calorimetry,[18] and thermal conductivity[19] can also be interpreted in terms of disorder of the hydrogen atoms of the water molecules.

For the guest component, X-ray diffraction studies at ambient temperature[11] located only a spherical shell of electron density, suggesting that the THF molecules undergo essentially unrestricted reorientational motions at this temperature. More recently, the crystal structure has been re-determined[13] from powder neutron diffraction data at low temperatures (80 and 5 K), providing evidence for preferred orientations of the THF molecules in the water cages at these temperatures.

In this paper, solid-state ^{2}H NMR spectroscopy has been used to investigate the dynamic properties of the water molecules in the THF clathrate hydrate [for samples containing deuterated water (THF−D_2O)] and the dynamic properties of the THF guest molecules [for samples containing perdeuterated THF (denoted TDF−H_2O)].

A number of previous NMR studies have also addressed dynamic aspects of the THF clathrate hydrate, mainly focusing on ^{1}H NMR techniques.[12,16,20,21] For THF−D_2O, the dependence of the ^{1}H NMR spin−lattice relaxation rate on inverse temperature was found to be asymmetric. This behavior has been modeled successfully for temperatures up to at least 150 K using a broad distribution of correlation times for the reorientation of the guest molecules, with a low activation energy (4.1 kJ mol^{-1} [12]). The reorientational motion of the water molecules was reported to be considerably slower than that of the guest molecules, with a higher activation energy (30.1 kJ mol^{-1} [16]).

A ^{2}H NMR study has also been reported previously,[17] involving measurement and analysis of ^{2}H NMR relaxation times at temperatures up to ca. 273 K. Measurements of ^{2}H NMR line shapes at a few very low temperatures (up to 56 K) were also reported. The discussion focused mainly on the dynamic properties of the host and guest components at low temperatures, below about 150 K. In this regard, the present paper represents a complementary ^{2}H NMR investigation, in which we focus on dynamic properties in a higher-temperature regime (above ca. 150 K). In particular, our studies of the dynamics of the water molecules in this temperature range are concerned largely with ^{2}H NMR line shape analysis, including fitting simulated spectra for several dynamic models to the experimental spectra (which was not carried out in the earlier paper[17]), leading to a more detailed structural interpretation of the dynamic properties of the water molecules. We also report ^{2}H NMR results for perdeuterated THF guest molecules at temperatures between 125 and 243 K, focusing both on ^{2}H NMR line shape analysis and ^{2}H NMR spin−lattice relaxation time measurements. Our studies at these temperatures point toward relationships between dynamic aspects of the host and guest components, even though the dynamics of these components occur on substantially different characteristic time scales.

^{2}H NMR studies of the dynamic properties of clathrate hydrates containing other guest molecules have also been reported.[22]

2. Background to ^{2}H NMR

A nucleus with spin (I) greater than $^1/_2$ has an electric quadrupole moment, which interacts with the electric field gradient at the nucleus. For the ^{2}H nucleus (for which $I = 1$), the quadrupolar interaction is usually the dominant anisotropic nuclear spin interaction in the solid state. The NMR spectrum of a ^{2}H nucleus in a solid depends on the electric field gradient tensor ($\mathbf{V}$) at the nucleus. In the principal axis system, the principal components of the electric field gradient tensor ($\mathbf{V}^{PAS}$) are taken such that $|V_{zz}| \geq |V_{yy}| \geq |V_{xx}|$. The quadrupole coupling constant χ is defined as eQV_{zz}/h (where Q is the electric quadrupole moment of the nucleus), and the asymmetry parameter η is defined as $\eta = (|V_{yy}| - |V_{xx}|)/|V_{zz}|$ (note that η is in the range $0 \leq \eta \leq 1$). The z-axis of the $\mathbf{V}^{PAS}$ tensor lies close to the direction of the C−D bond in the case of the THF-d_8 molecule and close to the direction of the O−D bond in the case of the D_2O molecule, and in the present work, we assume that the z-axes of the $\mathbf{V}^{PAS}$ tensors are coincident with these bonds.

^{2}H NMR line shapes are sensitive to molecular motion in solids, particularly when the correlation time (τ_c) for the motion is in the range of 10^{-3}−10^{-7} s (the intermediate motion regime). In this regime, the ^{2}H NMR line shape depends critically on the mechanism and rate of motion. For correlation times shorter than 10^{-7} s (rapid motion regime), the actual rate of motion cannot be established from ^{2}H NMR line shape analysis, but information on the geometry and mechanism of the motion can nevertheless be obtained. For correlation times longer than 10^{-3} s (static/slow motion regime), the ^{2}H NMR line shape is insensitive to the occurrence of the motion, and a line shape characteristic of a static system is observed. ^{2}H NMR line shape analysis is generally carried out by calculating the line shapes for proposed dynamic models and by finding the dynamic model for which the set of calculated line shapes provides the best fit to the set of experimental line shapes recorded as a function of temperature. When the rate of motion is in the rapid regime with respect to ^{2}H NMR line shape analysis, detailed dynamic information can be obtained from measurement and analysis of the ^{2}H NMR spin−lattice relaxation time (T_1), which is particularly sensitive for studying dynamic processes with

correlation times in the range $10^{-3}/\nu$ to $10^{3}/\nu$ (where ν is the ^{2}H Larmor frequency).

3. Experimental Section

3.1. Sample Preparation. The THF clathrate hydrate (denoted THF−D_2O) containing deuterated water was prepared by crystallization from a mixture of D_2O and THF in the molar ratio 16.9/1. The THF clathrate hydrate (denoted TDF−H_2O) containing perdeuterated THF was prepared by crystallization from a mixture of H_2O and THF-d_8 (denoted TDF) in the molar ratio 16.9/1. The flasks containing the solutions were immersed in a cold bath at 273 K and were left for 6 h to allow crystallization to occur. In some cases, the solution was perturbed with a spatula in order to induce crystallisation.

For ^{2}H NMR experiments, the samples were gently crushed and quickly packed into a glass tube under a dry nitrogen atmosphere to prohibit isotopic exchange with atmospheric H_2O (particularly for the THF−D_2O sample). All handling of samples was carried out in a cold room maintained below the melting temperature (277.4 K) of the THF clathrate hydrate.[23] After the samples were packed for the ^{2}H NMR experiments, they were immersed in liquid nitrogen and transferred rapidly to the NMR spectrometer.

3.2. ^{2}H NMR. ^{2}H NMR spectra were recorded for polycrystalline samples of THF−D_2O and TDF−H_2O at 46.08 MHz on a Chemagnetics CMX Infinity 300 spectrometer using a static probe (with 5 mm diameter coil). The standard quadrupole echo $[(90°)_\phi-\tau-(90°)_{\phi\pm\pi/2}-\tau'-$acquire−recycle] pulse sequence[24] was used, with a 90° pulse duration of 2 μs and an eight step phase cycle. Separate spectra were recorded for two different values ($\tau = 30$ μs and $\tau = 120$ μs) of the echo delay. The accuracy of the temperature controller used in this work was ca. ± 2 K, and the stability was ca. ± 0.2 K.

For THF−D_2O, quadrupole echo ^{2}H NMR spectra were recorded in the temperature range of 153−263 K using recycle delays ranging from 7 to 1200 s, depending on the temperature. For TDF−H_2O, quadrupole echo ^{2}H NMR spectra were recorded in the temperature range of 125−243 K, with recycle delays ranging from 10 to 18 s, depending on the temperature. For each temperature, the recycle delay was longer than 5 times the estimated value of T_1.

Simulations of ^{2}H NMR powder line shapes for proposed dynamic models were carried out using the program MXQET.[25]

^{2}H NMR spin−lattice relaxation times (T_1) were measured using the saturation recovery technique between 233 and 263 K for THF−D_2O and between 143 and 213 K for TDF−H_2O. Saturation recovery experiments were recorded using the pulse sequence $\{[\tau_d-(180°)_x]_n-\tau_r-(90°)_\phi-\tau-(90°)_{\phi\pm\pi/2}-\tau'-$acquire−recycle}, where $n = 30$, $\tau_d = 100$ μs for THF−D_2O and 10 μs for TDF−H_2O, $\tau = 30$ μs, and $\tau_r = t_o[(10)^{1/10}]^{N-1}$ (in this expression, t_o is the duration of the first delay, and N is the delay number). Fitting of the saturation recovery data by single or double exponential recovery functions was carried out using the spectrometer software.

Inversion recovery spectra were recorded for TDF−H_2O at 173 K using an inversion recovery pulse sequence modified for ^{2}H nuclei.[26] This pulse sequence comprises a composite inversion pulse followed by quadrupole echo detection $\{[(CP)(\overline{CP})(CP)]_\varphi-\tau_r-(90°)_\phi-\tau-(90°)_{\phi\pm\pi/2}-\tau'-$acquire−recycle}, where $\tau = 30$ μs and (CP) ≡ 17°, 62°, 99°, 144° (overbar indicates 180° phase shift).

For TDF−H_2O, ^{2}H NMR spin−spin relaxation behavior in the temperature range of 128−213 K was investigated using the standard quadrupole echo pulse sequence with a variable inter-pulse delay τ.

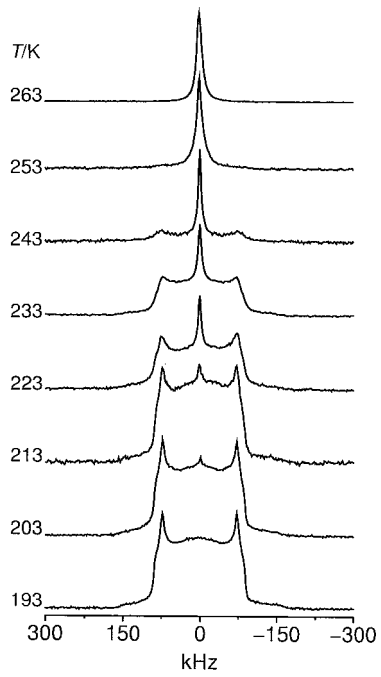

Figure 2. Experimental ^{2}H NMR spectra of THF−D_2O recorded as a function of temperature using the quadrupole echo pulse sequence with $\tau = 30$ μs.

4. Dynamics of the Water Molecules in THF−D_2O

^{2}H NMR spectra recorded for THF−D_2O in the temperature range of 193−263 K are shown in Figure 2. The ^{2}H NMR line shape changes from a relatively narrow single line at high temperatures (253−263 K) to a characteristic static ^{2}H NMR powder pattern at 193 K and lower temperatures. Note that the hump observed in the center of the spectrum at these low temperatures is attributed to a feature of the probe used and is reproduced in simulations of the ^{2}H NMR spectra by treating the 90° pulse length as a variable parameter. From ^{2}H NMR spectra recorded for different values of the echo delay [$\tau = 30$ and 120 μs (not shown)], the ^{2}H NMR line shape depends significantly on the echo delay at temperatures above 193 K, suggesting that the dynamic processes are in the intermediate motion regime throughout this temperature range.

Several different dynamic models have been considered in simulations of the ^{2}H NMR line shapes. All models are based on a tetrahedral arrangement of ^{2}H sites, consistent with the time-averaged spatial distribution of the deuterons of a D_2O molecule interacting with each of its four neighboring D_2O molecules by O−D···O hydrogen bonds (as in the known crystal structure discussed in section 1). Thus, the oxygen atom of a given D_2O molecule is located at the center of a tetrahedron, and the deuteron sites are located at the vertexes (Figure 3). The dynamic models involve jumps of the deuterons of a given D_2O molecule between these sites, with details given below. In all cases, the four sites were taken to have equal populations. The quadrupole interaction parameters determined by fitting the static line shape at 193 K are $\chi = 215$ kHz and $\eta = 0.1$, and these values were used as the static quadrupole interaction parameters in the line shape simulations at all other temperatures. We note that these values of χ and η are close to those reported previously for polycrystalline[27] and single crystal[28] samples of hexagonal ice.

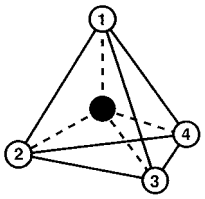

Figure 3. Specification of the deuteron sites involved in the four-site tetrahedral jump model. The oxygen atom of the D_2O molecule (filled circle) remains at the center of the tetrahedron. The two deuterons of the D_2O molecule can occupy any of the 4 sites shown with equal probabilities.

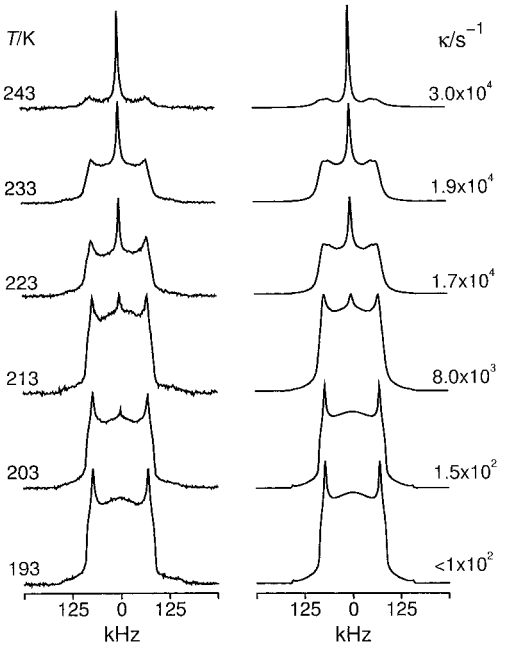

Figure 4. Experimental and best-fit simulated ^2H NMR spectra for the D_2O molecules in THF−D_2O, with the simulated spectra calculated using model A1. The jump rate (κ) used to simulate each spectrum is indicated.

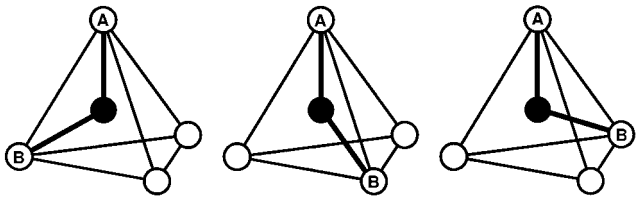

Figure 5. Scheme showing 3 of the 12 different orientations of the D_2O molecule considered in model A2. Although deuteron A occupies the same site in each of the 3 different orientations, the orientation of the $\mathbf{V}^{PAS}$ tensor for this deuteron is different in each case, on account of the different location of deuteron B and the fact that $\eta \neq 0$ for the deuterons in D_2O.

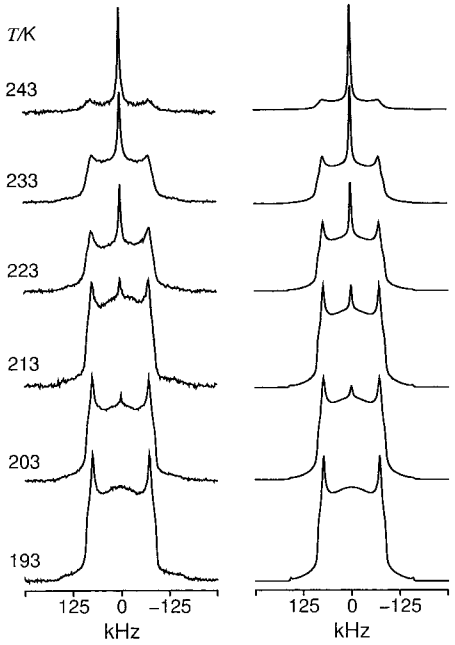

Figure 6. Experimental and best-fit simulated ^2H NMR spectra for the D_2O molecules in THF−D_2O, with the simulated spectra calculated using model B2. The jump rates (κ_1 and κ_2) of components 1 and 2 used to calculate each simulated spectrum are given in Table 1.

Model A1 comprises a single component of motion involving four tetrahedral sites with equal populations. Simulated ^2H NMR spectra for this model are compared with the experimental ^2H NMR spectra in Figure 4. This model provides a reasonable fit to the experimental spectra at 213 K and lower temperatures. However, at higher temperatures, there are significant discrepancies between experimental and simulated line shapes, and above 253 K, the model cannot produce a single line as broad as the experimental line shape.

Model A2 comprises a single component of motion involving 12 types of sites with equal populations. Structurally, these 12 sites represent 4 positions at the vertexes of a tetrahedron, but for each of these positions of the ^2H nucleus there are 3 different orientations of the $\mathbf{V}^{PAS}$ tensor. These three different orientations are not equivalent as a consequence of the fact that $\eta \neq 0$. Thus, in Figure 5, the orientation of the $\mathbf{V}^{PAS}$ tensor for deuteron A strictly depends on the position of deuteron B. For model A2, jumps are not possible between all pairs of sites, and a restricted set of allowed jumps was used. Although this model is fundamentally different from model A1, the simulated powder ^2H NMR line shapes are actually very similar to those obtained using model A1.

Model B comprises two independent components, each of which undergoes the four-site tetrahedral jump motion (involving four sites with equal populations) described above for model A1, but with independent jump rates. The component with lower jump rate is denoted 1, and the component with higher jump rate is denoted 2. For a given series of simulations, the relative numbers (populations) of D_2O molecules representing components 1 and 2 were fixed, as now described. The crystal structure of the THF clathrate hydrate[11,13] contains three crystallographically different types of water molecule in the ratio of 1:4:12. There is no constraint (crystallographically) that these three types of D_2O molecule must have the same dynamic properties. The contribution of the first type of water molecule to the ^2H NMR line shape is neglected because of its low relative population, and the other two types of water molecule may be considered in the dynamic model with populations in the ratio of 1:3. In model B1, the component with lower population has the lower jump rate (component 1), whereas in model B2 the component with lower population has the higher jump rate (component 2). For comparison, another model (Model B3) was also considered in which the populations of components 1 and 2 are equal. For models B1, B2, and B3, simulated ^2H NMR spectra (with the jump rates of components 1 and 2 varied and the relative populations fixed) are in good agreement with the experimental ^2H NMR spectra at 243 K and lower temperatures (Figure 6). The jump rates for the best fit simulations are given in Table 1.

Comparison of the experimental and best-fit simulated spectra at each individual temperature does not lead to a clear discrimination between models B1, B2, and B3, as in all cases

TABLE 1: Jump Rates κ_1 and κ_2 (for components 1 and 2 respectively) Obtained from Best Fit Simulations of Models B1, B2, and B3 to the Experimental ^{2}H NMR Spectra for THF−D_2O as a Function of Temperature[a]

	model B1		model B3		model B2	
T/K	κ_1/s	κ_2/s	κ_1/s	κ_2/s	κ_1/s	κ_2/s
243	1.0×10^4	1.9×10^5	1.0×10^4	6.4×10^5	1.0×10^4	1.7×10^6
233	6.0×10^3	7.0×10^4	5.0×10^3	2.8×10^5	4.9×10^3	7.6×10^5
223	1.25×10^3	1.25×10^5	2.0×10^3	2.4×10^5	2.2×10^3	8.0×10^5
213	5.0×10^2	4.0×10^4	7.3×10^2	1.0×10^5	2.0×10^3	2.0×10^5
203	1.0×10^2	1.9×10^4	2.7×10^2	5.0×10^4	4.0×10^2	1.0×10^5
populations	p_1	p_2	p_1	p_2	p_1	p_2
	0.25	0.75	0.5	0.5	0.75	0.25

[a] The relative populations (p_1 and p_2) of components 1 and 2 were fixed in each model at the values indicated. For all simulations, the static quadrupole interaction parameters were taken as $\chi = 215$ kHz and $\eta = 0.1$

good agreement is found (we note that, as both components are in the intermediate motion regime in the temperature range of 203−263 K, it is harder than otherwise to estimate the relative populations of the two components accurately by ^{2}H NMR). However, the best fits for each model represent different jump rates (denoted κ_1 and κ_2) at each temperature, as shown in Table 1. In all cases, graphs of $\ln(\kappa_i/s^{-1})$ versus T^{-1}/K^{-1} show linear behavior, allowing activation energies to be estimated on the assumption of Arrhenius behavior [$\kappa_i = A \exp(-E_a/RT)$] for the temperature dependences of κ_1 and κ_2. The activation energies differ significantly between model B1 (48 and 23 kJ mol^{-1} for components 1 and 2 respectively), model B2 (31 and 28 kJ mol^{-1}), and model B3 (37 and 25 kJ mol^{-1}). For comparison, previous determinations of the activation energy have been 30.1 kJ mol^{-1} from solid-state ^{1}H NMR studies[16] and 30.9 kJ mol^{-1} from dielectric studies.[29] These results are in closest agreement with the activation energies obtained here for model B2. We note that the activation energy (56.5 kJ mol^{-1}) obtained from ^{2}H NMR line shape studies of hexagonal ice[27] is significantly higher than the values obtained for THF−D_2O.

We now assess whether differences in the activation energies for components 1 and 2 in the THF clathrate hydrate may relate to differences in structural properties (particularly differences in intermolecular interactions) for the different types of water molecule in the host structure.[11,13] In fact, the water molecules with higher and lower populations have very similar O···O hydrogen bond distances[30]—the water molecule of higher population has O···O distances to the four adjacent water molecules of ca. 2.76 Å, whereas the water molecule of lower population has three O···O distances of ca. 2.72 Å and one O···O distance of ca. 2.76 Å. Thus, it is reasonable to speculate that the local interactions involving the water molecules of higher and lower populations do not differ substantially (while recognizing that caution is required before assuming that hydrogen bond distances are a direct indication of hydrogen bond interaction strengths). This situation appears to be most consistent with the results of model B2, for which the activation energies of components 1 and 2 are closest to each other.

Our conclusion that there are at least two dynamically distinguishable types of water molecules is in agreement with results from dielectric studies,[29] for which two discrete relaxation times were found. In these studies, the slower component was assigned to have the higher population, similar to our model B2, although the dielectric studies suggested that the ratio of the populations is 2:1 (in contrast to the 3:1 ratio expected on the basis of the crystal structure).

At 253 and 263 K, the experimental ^{2}H NMR spectrum may be described as a single line and is consistent in qualitative terms with model B, provided that the jump rates of both components are greater than ca. 4×10^4 s^{-1}. However, the width of the experimental line shape at these temperatures is too broad to be simulated adequately by the dynamic models discussed above. This discrepancy between experimental and simulated line shapes may suggest that additional dynamic features become important at these temperatures. It is relevant to note that these temperatures are relatively close to the melting temperature of the material.

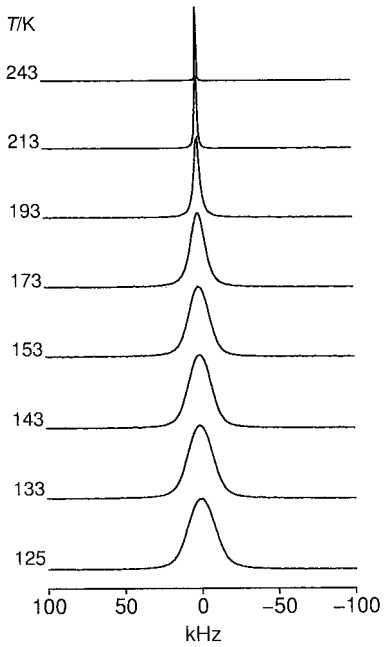

Figure 7. Experimental ^{2}H NMR spectra of TDF−H_2O recorded as a function of temperature using the quadrupole echo pulse sequence with $\tau = 30$ μs.

Measurements of ^{2}H NMR spin−lattice relaxation times were also carried out in the temperature range of 233−263 K, in part to assess the recycle delays to be used in our ^{2}H NMR line shape studies discussed above. Attempts were made to fit the spin−lattice relaxation time data to single and double exponential recovery functions. For the lowest temperature (233 K), the data were clearly better fitted by two components (with T_1 differing by about 2 orders of magnitude) in support of conclusions discussed above for this temperature range. At temperatures higher than 233 K, it was ambiguous whether the data were fitted better by a single or double exponential recovery function.

5. Dynamics of the Guest Molecules in TDF−H_2O

^{2}H NMR spectra recorded for TDF−H_2O in the temperature range of 125−243 K are shown in Figure 7 and comprise a single line at each temperature. The observed width of the line

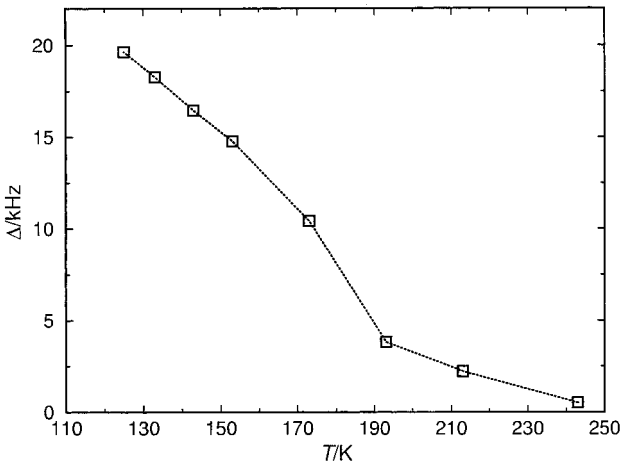

Figure 8. Experimental line width (Δ, full width at half-maximum) as a function of temperature for the single line in the ^{2}H NMR spectrum of TDF−H_2O.

decreases as temperature is increased (see Figure 8), ranging from about 20 kHz (full width at half-maximum) at 125 K to about 2 kHz at 243 K. At 125 K, the line shape is virtually a pure Gaussian, but at higher temperatures, the line shape is described by a pseudo-Voigt function with increasing Lorentzian character as temperature is increased. The fact that a single line is observed throughout the temperature range is consistent with the TDF molecules undergoing isotropic (or close to isotropic) reorientational motion in the rapid motion regime with respect to ^{2}H NMR line shape analysis. However, simulations of the ^{2}H NMR spectrum using an isotropic model are unable to reproduce the substantial increase in the experimental line width on decreasing temperature, particularly below 213 K. The line shape is independent of echo delay ($\tau = 30$ and 120 μs) at each temperature from 125 to 243 K, supporting our assignment that the motion is in the rapid regime (the fact that there is no significant variation of the intensity of the echo maximum as a function of temperature also supports this assignment). The substantial broadening of the spectrum on decreasing temperature may indicate that the motion either acquires some anisotropic character or a distribution of correlation times, as discussed in more detail below. An increase in the anisotropic character may arise, for example, from local structural differences in the geometries of different cages.

We now consider the ^{2}H NMR spin−lattice relaxation behavior of TDF−H_2O, recalling that this approach can provide more quantitative insights concerning the rates of dynamic processes that are in the rapid regime with respect to ^{2}H NMR line shape analysis. ^{2}H NMR spectra recorded using the inversion recovery pulse sequence at 173 K are shown in Figure 9, from which it is clear that all parts of the spectrum exhibit the same spin−lattice relaxation behavior. Furthermore, ^{2}H NMR saturation recovery data for TDF−H_2O can be fitted by a single-exponential recovery function throughout the temperature range studied (143−213 K) suggesting that the relaxation of all deuterons in the sample is caused by the same motion with a single correlation time. In contrast, previous ^{2}H NMR studies[17] at lower temperatures suggest that there is a distribution of correlation times—this issue is discussed below.

From the fit to the saturation recovery data, the powder average of the reciprocal of the ^{2}H NMR spin−lattice relaxation time (denoted $\langle 1/T_1\rangle_p$) can be determined. As shown in Figure 10, a plot of $\ln[(\langle 1/T_1\rangle_p)^{-1}/\mathrm{s}]$ versus T^{-1}/K^{-1} is linear, and the negative gradient indicates that the motion causing the relaxation is in the extreme narrowing regime ($\tau_c \lesssim 10^{-9}$ s). On the

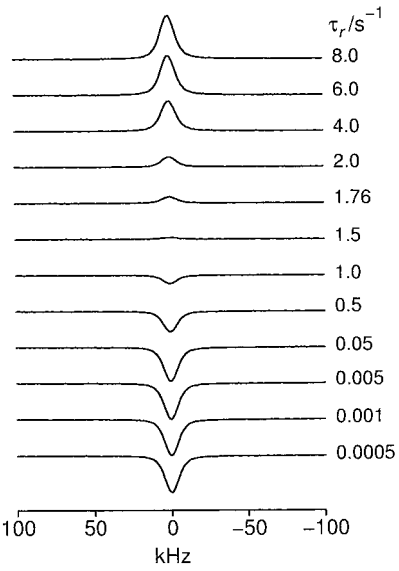

Figure 9. ^{2}H NMR spectra recorded for TDF−H_2O at 173 K using the inversion−recovery technique as a function of the recovery time τ_r.

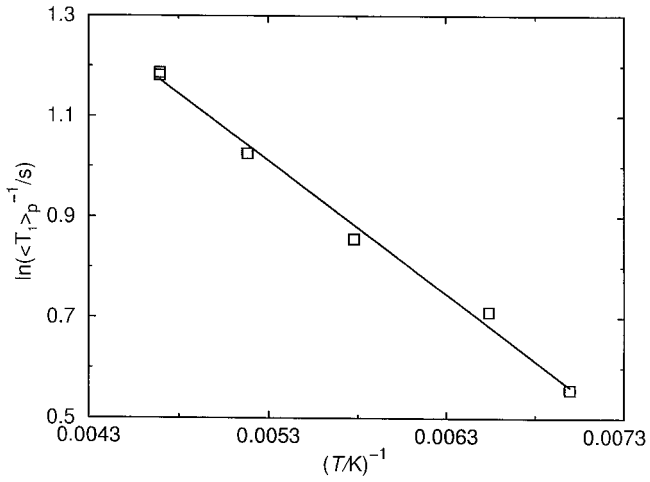

Figure 10. ^{2}H NMR spin−lattice relaxation time data for TDF−H_2O, plotted as a graph of $\ln[(\langle 1/T_1\rangle_p)^{-1}/\mathrm{s}]$ versus T^{-1}/K^{-1}.

assumption of Arrhenius behavior [$\tau_c = \tau_o \exp(E_a/RT)$], the activation energy for the reorientation of the guest molecules is estimated from Figure 10 to be 2.2 kJ mol^{-1}. For comparison, the activation energy reported previously[16] from solid-state ^{1}H NMR studies is 3.85 kJ mol^{-1}.

In the temperature range studied here, our ^{2}H NMR line shape analysis suggests that there is a distribution in terms of the dynamic behaviors of different TDF molecules, although our ^{2}H NMR spin−lattice relaxation time studies indicate that this does not represent a distribution of correlation times for the motion. Instead, we may infer that there is a distribution of geometries for the motion, and we propose that the motion acquires some anisotropic characteristics at the lower temperatures studied here, with a distribution in terms of the exact nature of the anisotropy. Thus, the distribution of dynamic behavior concerns the deviation from isotropic motional geometry rather than the correlation time for this motion, such that the spin−lattice relaxation time data are well represented by a single component.

From the structural viewpoint, this situation implies a range of different local environments for the THF molecules in the structure. As discussed above, the reorientation of the water

molecules of the host structure is in the slow or intermediate motion regime and is therefore slower by several orders of magnitude than the reorientation of the THF molecules. Thus, on the time scale of the reorientation of the THF molecules ($\tau_c \lesssim 10^{-9}$ s), the water cage appears static, and the exact local geometries of the cages will differ from cage to cage depending on the specific configuration of O−H···O hydrogen bonds in the cage. On a time average and/or space average (as probed by diffraction measurements), all cages occupied by THF molecules are identical, but because of the motion of the water molecules, different THF molecules effectively experience different local cage geometries when considered over a sufficiently short time scale. In particular, while the geometry of the cage is very close to spherical in the average structure determined from diffraction studies, the actual geometry of the cage considered over a sufficiently short time scale (on the order of the correlation time for the motion of the guest molecules) may differ appreciably from spherical geometry, particularly at lower temperatures. The resultant distribution of nonspherical local geometries of the cages should clearly give rise to a distribution of dynamic properties of the THF molecules in terms of dynamic models that may be close to isotropic but exhibiting a distribution of anisotropic characteristics. We note that it is completely plausible from the physicochemical viewpoint, particularly at sufficiently high temperature, to have a situation in which guest molecules in different host−guest potentials (arising, for example, from having different local cage geometries as discussed above) undergo motions with different geometric characteristics but with effectively the same correlation time. However, on decreasing temperature, it may be expected that the different host−guest potentials may give rise to distributions in both the geometric characteristics and correlation times of the motion of the guest molecules.

Additional evidence relating to the issues discussed above is obtained from ^{2}H NMR quadrupole echo spectra recorded with a variable interpulse delay. Such spectra recorded for TDF−H_2O between 128 and 213 K can be fitted only by a Gaussian decay function with three or more components. One interpretation is that there is more than one type of spin−spin relaxation behavior of the THF molecules, consistent with a distribution of dynamic characteristics and suggesting that the observed ^{2}H NMR line shape is actually inhomogeneous. This conclusion is clearly consistent with the above discussion.

Finally, it is interesting to note that the observed line width in the ^{2}H NMR spectrum of TDF−H_2O exhibits a particularly significant decrease at temperatures leading up to ca. 190 K (see Figure 8) and that this temperature region coincides with the motion of the water molecules entering the intermediate motion regime with respect to ^{2}H NMR line shape analysis (see Figure 6). In view of our proposal that the distribution of the dynamic properties of different guest molecules may be related to the fact that different water cages have different local geometries over a sufficiently short time scale, it is perhaps not surprising that the distribution in the dynamic properties of different guest molecules should narrow substantially when the motion of the water cages enters the regime in which ^{2}H NMR line shapes become influenced by the motion. Thus, while the time scale for the reorientation of the THF guest molecules is substantially shorter than the time scale for the motion of the water molecules, the distribution in terms of the anisotropies of the motions of different THF guest molecules may nevertheless change on the same time scale as that of the motion of the water molecules.

6. Concluding Remarks

Our ^{2}H NMR studies have produced a number of new insights concerning dynamic properties of the THF clathrate hydrate. For the host structure, at least two dynamically distinguishable types of water molecule are identified, both undergoing a four-site tetrahedral jump motion but with different rates. The dynamics of both components are in the intermediate motion regime with respect to ^{2}H NMR line shape analysis above 193 K, allowing the jump rates to be determined as a function of temperature and allowing activation parameters to be established. Our interpretation of the dynamic properties of the water molecules has been based on knowledge of the host structure, recognizing that a necessary requirement for assigning a correct dynamic model is that the time average of the model must agree with the crystal structure determined from diffraction data.

^{2}H NMR spectra of the THF guest molecules are interpreted in terms of a motion that is close to isotropic and in the rapid motion regime, but with a distribution of anisotropic characteristics, which changes as a function of temperature. As the THF molecules reorient rapidly in comparison with the dynamics of the water molecules, each THF molecule is surrounded by a slightly different water cage, and the resultant distribution of local cage geometries confers differing degrees of anisotropic character on the reorientational motions of different THF molecules in the structure. Although different water cages have different anisotropic characteristics (when considered on the time scale of the motion of the THF guest molecules), the motions of the THF molecules in different water cages can be described well by a single correlation time (or a sufficiently narrow distribution of correlation times, consistent with the experimental errors inherent in fitting the ^{2}H NMR spin−lattice relaxation data). We note that, as the motion of the THF molecules is in the rapid regime, the ^{2}H NMR line shape analysis is unable to address the question of whether there are any differences in the correlation times for the THF molecules in different water cages.

Although some aspects of the dynamic properties determined from our ^{2}H NMR studies are in apparent contradiction with conclusions from previous work,[17] these differences may be reconciled by recognizing that our studies have focused on a higher-temperature regime (above ca. 150 K) than the previous study. In particular, our studies provide a more detailed structural interpretation of the dynamic properties and also point towards relationships between dynamic aspects of the host and guest components, even though the dynamics of these components occur on substantially different characteristic time scales.

Acknowledgment. We are grateful to EPSRC, HEFCE, and Ciba Specialty Chemicals for financial support. We thank O. Yamamuro for providing unpublished information on structural properties of the THF clathrate hydrate.

References and Notes

(1) Davy, H. *Philos. Trans. Royal Soc.* **1811**, *101*, 155.
(2) Franks, F. *Water - A Comprehensive Treatise*; Plenum Press: New York, 1973; Vol. 2.
(3) Sloan, E. D., Jr. *Clathrate Hydrates of Natural Gases*; Marcel Dekker Inc.: New York, 1990.
(4) Yamamuro, O.; Suga, H. *J. Therm. Anal.* **1989**, *35*, 2025.
(5) Koh, C. A.; Wisbey, R. P.; Wu, X.; Westacott, R. E.; Soper, A. K. *J. Chem. Phys.* **2000**, *113*, 6390.
(6) Ripmeester, J. A.; Ratcliffe, C. I.; Klug, D. D.; Tse, J. S. *Ann. N.Y. Acad. Sci.* **1994**, *715*, 161.
(7) Van Stackelberg, M.; Jahns, W. *Z. Elektrochem.* **1954**, *58*, 162.
(8) Müller, H. R.; Van Stackelberg, M. *Z. Elektrochem.* **1954**, *58*, 25.
(9) Jeffrey, G. A. In *Inclusion Compounds*; Atwood, J. L., Davies, J. E. D., MacNicol, D. D., Eds.; Academic Press: London, 1984; Vol. 1, pp 135−140.

(10) Ripmeester, J. A.; Tse, J. S.; Ratcliffe, C. I.; Powell, B. H. *Nature* **1987**, *325*, 135.
(11) McMullan, R. K.; Mak, T. C. W. *J. Chem. Phys.* **1965**, *42*, 2732.
(12) Albayrak, C.; Zeidler, M. D.; Küchler, R.; Kanert, O. *Ber. Bunsen-Ges. Phys. Chem.* **1989**, *93*, 1119.
(13) Yamamuro, O.; Matsuo, T.; Suga, H.; David, W. I. F.; Ibberson, R. M.; Leadbetter, A. J. *Phys. B* **1995**, *213*, 405.
(14) Davidson, D. W. In *Water - A Comprehensive Treatise*; Franks, F., Ed.; Plenum Press: New York, 1973; Vol. 2, p 115.
(15) Yamamuro, O.; Matsuo, T.; Suga, H. *J. Inclusion Phenom.* **1990**, *8*, 33.
(16) Ripmeester, J. A.; Garg, S. K.; Davidson, D. W. *J. Magn. Reson.* **1974**, *15*, 295.
(17) Ripmeester, J. A.; Garg, S. K.; Davidson, D. W. *J. Magn. Reson.* **1978**, *31*, 399.
(18) Yamamuro, O.; Oguni, M.; Matsuo, T.; Suga, H. *J. Phys. Chem. Solids* **1988**, *49*, 425.
(19) Andersson, O.; Suga, H. *J. Phys. Chem. Solids* **1996**, *57*, 125.
(20) Haywood, R. J.; Packer, K. J. *Mol. Phys.* **1973**, *25*, 1443.
(21) Jacobs, D. M.; Zeidler, M. D.; Kanert, O. *J. Phys. Chem. A* **1997**, *101*, 5241.
(22) Collins, M. J.; Ratcliffe, C. I.; Ripmeester, J. A. *J. Phys. Chem.* **1990**, *94*, 157.
(23) Davidson, D. W.; Gough, S. R. *Can. J. Chem.* **1971**, *58*, 25.
(24) Davis, J. H.; Jeffrey, K. R.; Bloom, M.; Valic, M. I.; Higgs, T. P. *Chem. Phys. Lett.* **1976**, *42*, 390.
(25) Greenfield, M. S.; Ronemus, A. D.; Vold, R. L.; Vold, R. R.; Ellis, P. D.; Raidy, T. R. *J. Magn. Reson.* **1987**, *72*, 89.
(26) Raleigh, D. P.; Olejniczak, E. T.; Griffin, R. G. *J. Magn. Reson.* **1989**, *81*, 445.
(27) Pines, A.; Wemmer, E. D.; Ruben, D. J.; Usha, M. G.; Wittebort, R. J. *J. Am. Chem. Soc.* **1988**, *110*, 5668.
(28) Waldestein, P.; Rabideay, S. W.; Jackson, J. A. *J. Chem. Phys.* **1964**, *41*, 3407.
(29) Gough, S. R.; Davidson, D. W.; Hawkins, R. E.; Morris, B. *J. Phys. Chem.* **1973**, *77*, 2969.
(30) Yamamuro, O. Personal communication, 1999.